III-V micro- and nano-lasers grown on silicon emitting in the telecom band

Kei May Lau, Yu Han, Si Zhu, Wei Luo, and Ying Xui

Department of Electronic and Computer Engr., Hong Kong University of Science and Technology, Clear Water Bay, Kowloon, Hong Kong

*eekmlau@ust.hk

Abstract: We present our recent effort on the integration of 1.5 µm III-V micro-cavity lasers on (001) Si wafers, and bufferless nano-lasers on (001) silicon-on-insulators (SOI) via direct hetero-epitaxy by metal organic chemical vapor deposition.

OCIS codes: (140.3410) Laser resonators; (140.3948) Microcavity devices; (230.5590) Quantum-well, -wire and -dot devices

1. Introduction

With recent demonstrations of competitive laser performances to their native III-V counterparts [1], III-V lasers directly grown on Si have reached the primary stage for a large-scale monolithic photonic integration platform from a techno-economic perspective. The capacity of scaling to 300 mm Si wafers in industry also warrants the feasibility of monolithic co-integration with micro-electronics. Following the "Moore's law" in photonic integrated circuits (PICs), there is a craving in down-sizing the footprint of these monolithically grown III-V-on-Si lasers for energy efficiency, dense integration and chip complexity. In this paper, we briefly summarize our approaches in such miniaturization, including high-quality whispering-gallery-mode (WGM) micro-cavity lasers through blanket III-V hetero-epitaxy on Si, and nano-ridge lasers by selective epitaxy on SOI. Challenges and opportunities of each approach are discusses in the following sections.

2. Micro-lasers grown on Si

WGM micro-lasers with disk or ring resonator geometries are one of the most attractive on-chip light sources for PICs. Their inherent traveling wave operation nature requires no gratings or cleaved facets for optical feedback. Self-assembled QDs, as emerging superior gain elements, offer unique characteristics of strong carrier localization in discrete three-dimensional nanostructures and less sensitivity to surface and interfacial defects. As a result, incorporating QDs promises a greater immunity to defects in III-V/Si hetero-epitaxy, and suppresses the severe spreading and surface recombination of non-equilibrium carriers in ultra-small lasers, leading to good device performance with low threshold and high temperature stability.

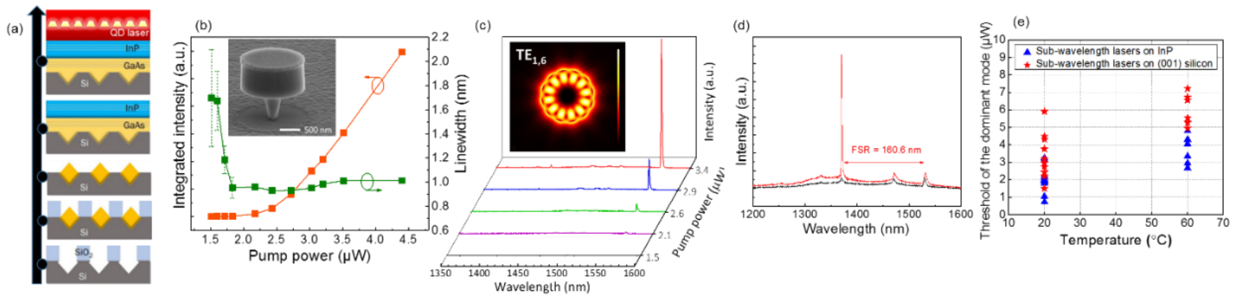

Fig.1 (a) Growth of QD lasers on V-grooved Si. (b) L-L curve and linewidth evolution of one 1.5 µm-diameter disk pumped by a 532 nm pulsed laser. (Insert: SEM image showing the device structure). (c) Lasing spectra, lasing mode identified to be $TE_{1,6}$. (d) Threshold comparison with 1.5 µm-diameter micro-disk lasers simultaneously grown and fabricated on InP at 20 °C and 60 °C.

Fig. 1 and Fig. 2 show the structures and some basic lasing characteristics of our optically pumped QD micro-disk lasers (MDL) and electrically-pumped micro-ring lasers on Si [2-4]. In these approaches, the laser cavities are formed through top-down fabrication steps using epitaxial blanket InP thin-film templates on patterned Si wafers, with the growth procedure schematically shown in Fig. 1(a). In the micro-disk laser structure (SEM in Fig. 1(b)), the fundamental WGM is tightly confined in both horizontal and vertical directions, enabling ultra-small device sizes in wavelength scales. We observed single-mode 1.55 µm lasing from disks 1.5-µm in diameter (Fig. 1(c)) and lasing at 1.37 µm in 1.2-µm-diameter disks (Fig. 1(d)). And the lasing threshold is around two times of the same size micro-disk lasers grown on InP native substrates. Such optically-injected ultra-small micro-disk lasers on Si can be integrated with other short-wavelength pumping sources to achieve multiple long-wavelength emissions in the telecom bands.

Making electrically-pumped MDL of similar size is difficult and superfluous since the current injection to the lasing mode would be extremely low, and the emission power would not reach a practical level. Instead, we made electrically-driven micro-ring lasers on Si with larger outer radius of 25 µm (Fig. 2(a)). The epitaxial structure and the fabrication steps are more complex than the optically-pumped micro-disk lasers. Details can be found in [5]. Good electrical contacts formation is indicated by a typical V-I property for a P-I-N diode with a turn-on voltage of 0.7 V (Fig. 2(b)). and a series resistance of 10 Ω. And decent room-temperature laser performances can be achieved (Fig. 2(c , d)).

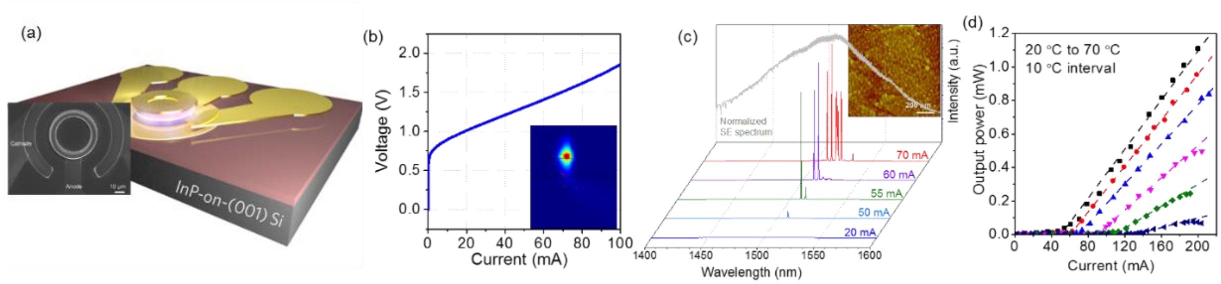

Fig. 2 (a) Device structure and top-down SEM image of the micro-ring laser on Si. (b) IV curve (insert: cross-sectional mode profile). (c) Lasing spectra at different currents, overlapped with the spontaneous emission (Insert: 1×1 µm^2 AFM image of the InAs/InAlGaAs QDs). (d) Temperature-dependent L-I curves under pulsed current injection.

Nevertheless, there is still plenty of room for improvement both in device performances and exploring efficient means for active/passive integration. Increasing the output power from unidirectional emission needs to be further investigated. Besides, controllable single-mode operation is crucial for practical WDM applications, and we have demonstrated our approach on InP [5]. As the micro-cavity lasers were built on InP/Si templates with a fairly thick buffer (a few microns), it's challenging to efficiently couple the above lasers with Si-based waveguides and other passive components.

3. Nano-lasers grown on SOI

In contrast to blanket epitaxial III-V thin films on Si with thick buffer layers and a dislocation density in the order of 10^6 cm^{-2} for GaAs and 10^8 cm^{-2} for InP, selectively grown III-V alloys on Si feature a bufferless attribute and are generally dislocation-free due to the unique growth mechanisms and the defect necking effects [6]. The intimate positioning of the epitaxial III-V and the Si substrate also facilitates efficient light coupling from the III-V active devices into Si-based passive components.

Our nano-lasers on bufferless InP/InGaAs nano-ridges were selectively grown on (001)-oriented SOI wafers. Epitaxy inside the V-grooved Si pockets with two {111} facets eliminates the formation of anti-phase boundaries [7]. Lattice mismatch between InP and Si is mainly accommodated by the formation of planar defects at the III-V/Si interface, while occasionally generated threading dislocations terminate at the oxide sidewalls (see Fig. 3(a)) [8-9]. Therefore, the upper epitaxial InP is essentially dislocation-free and is employed as the buffer layer for the growth of InGaAs/InP active regions. Fig. 3(b) presents a SEM image of the as-grown in-plane InP/InGaAs nano-ridges on SOI. Fig. 3(c) displays the cross-sectional TEM photo of one nano-ridge, manifesting the confinement of crystalline defects at the III-V/Si interface. The inserted InGaAs/InP ridge quantum wells feature an atomic sharp interface as shown in Fig. 3(d) [10].

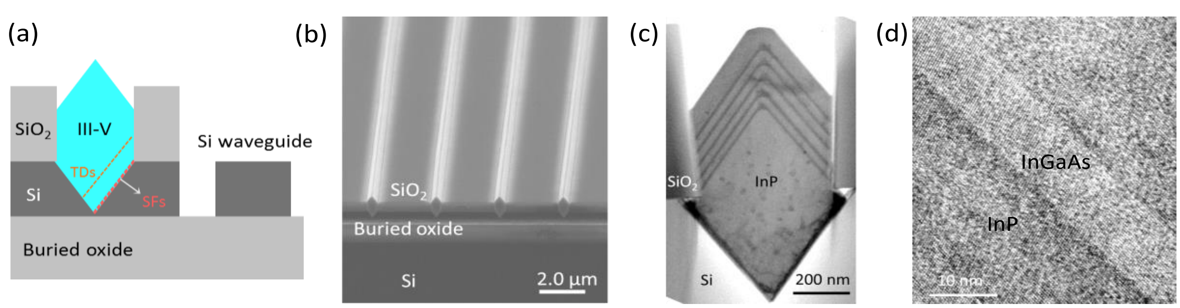

Fig. 3. (a) Schematic showing the selective growth of bufferless III-V nano-ridges on SOI wafers. (b) SEM image of the as-grown nano-ridges on SOI. (c) Cross-sectional TEM image of one nano-ridge, showing the formation of planar defects at the III-V/Si interface. (d) High-resolution TEM photo of one InP/InGaAs ridge quantum well with atomic sharp interfaces.

Simulated emission inside these nano-ridges demands a strong mode confinement within the epitaxial InP. Oxide spacers were thus removed, followed by undercutting Si into triangle-shaped pedestals and the definition of two end-facets (Fig. 4(a)). The fabricated InP/InGaAs nano-laser array is imaged in Fig. 4(b). Under optical pumping, we observed room temperature stimulated emission from these nano-lasers [11-12]. Fig. 4(c) plots the emission spectra of one nano-laser with a 60 µm cavity length. Below threshold, abroad spontaneous spectra appear with evenly-spaced resonance modes, while above threshold, a sharp peak at 1509 nm protrudes from the clamped background emission. The evolution of the peak intensity and line-width with the excitation levels is plotted in Fig. 4(d). The inset shows the simulated profile of the lasing TE_{01} mode. The threshold of the probed nano-lasers are around 40 µJ/cm^2.

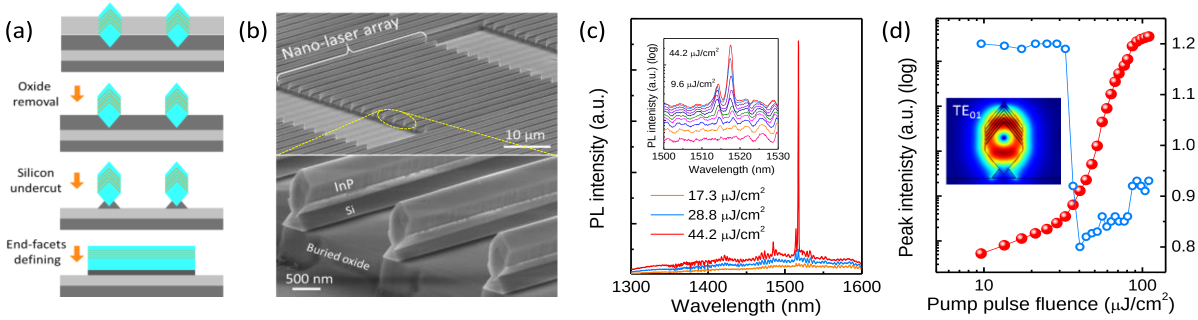

Fig. 4. (a) Schematic showing the fabrication process of nano-lasers on SOI. (b) Tilted-view SEM image of the fabricated nano-lasers on SOI. (c) Room temperature emission spectra of one nano-laser under optical pumping. (d) The evolution of the peak intensity and the line-width as the excitation level increases. Inset shows the modes profiles at 1500 nm.

The challenge regarding the bufferless nano-lasers is how to transcend from optical pumping to electrical injection. Although doping the epitaxial III-V nano-ridges can be readily achieved, a special technique must be developed to pattern the metal pads in a way that provides an efficient carrier injection, and, at the same time, ensures a minimal optical loss. Novel growth schemes are also required to grow III-V alloys with a larger material volume for flexible laser designs. Another imminent issue to tackle concerns the design of efficient interfacing between the epitaxial III-V light sources and the Si-based passive components.

4. Conclusion

In conclusion, we demonstrated 1.5 µm III-V micro-cavity lasers and nano-lasers directly grown on Si using two different approaches. The micro-ring/disk lasers built on blanket epitaxial InP thin films on Si, employs quantum dots as active gain medium to mitigate the influence of threading dislocations. The bufferless nano-lasers built on selectively epitaxial InP nano-ridges on SOI, adopt quantum wells as the active gain medium. These epitaxial III-V lasers on Si could serve as compact light sources in future fully integrated Si-based PICs.

Acknowledgement

The authors would like to thank RGC and ITF for supporting the research.

References

[1] D. Jung, R. Herrick, J. Norman, K. Turnlund, C. Jan, K. Feng, A. C. Gossard, and J. E. Bowers, Applied Physics Letters, vol. 112, no. 15, pp. 153507, (2018).

[2] S. Zhu, B. Shi, Q. Li, and K. M. Lau, Applied Physics Letters, vol. 113, no. 22, pp. 221103, (2018).

[3] S. Zhu, B. Shi, and K. M. Lau, Optics letters, vol. 44, no. 18, pp. 4566-4569, 2019.

[4] S. Zhu, B. Shi, Q. Li, Y. Wan, and K. M. Lau, Opt Express, vol. 25, no. 25, pp. 31281-31293, Dec 11, (2017).

[5] S. Zhu, X. Ma, W. Luo, B. Shi, and K. M. Lau, 2019 European Conference on Optical Communication (ECOC), Dublin, 2019.

[6] B. Shi, Y. Han, Q. Li, and K.M. Lau. IEEE Journal of Selected Topics in Quantum Electronics, 25(6), 1-11 (2019).

[7] Q. Li, K. W. Ng, and K. M. Lau, Appl. Phys. Lett., 106, 072105, (2015).

[8] Y. Han, Q. Li, S.P. Chang, W.D. Hsu, and K.M. Lau, Appl. Phys. Lett. 108, 242105 (2016).

[9] Y. Han, Q. Li, Si Zhu, Kar Wei Ng, and K.M. Lau, Appl. Phys. Lett. 111, 212101 (2017).

[10] Y. Han, W. K. Ng, C. Ma, Q. Li, S. Zhu, C. C. S. Chan, K. W. Ng, S. Lennon, R. A. Taylor, K. S. Wong, and K. M. Lau, Optica 5(8), 918 (2018).

[11] Y. Han, W. K. Ng, Y. Xue, Q. Li, K. S. Wong, and K. M. Lau, Opt. Lett. 44(4), 767(2019).

[12] Y. Han, W. K. Ng, Y. Xue, K. S. Wong, and K. M. Lau, Photonics Research 7(9), 1081-1086 (2019).